VOL.40 Nº2 2023
https://doi.org/10.22491/rmct.v40i2.11327.en

Ballistic resistance and microwave absorbing properties of a composite made of aramid fabric impregnated with polyethylene glycol and hematite nanoparticles

Danúbia Bordim de Carvalho[1*]
[1]**Military Institute of Engineering --Praça General Tibúrcio, 80, Praia Vermelha, Rio de Janeiro, RJ, Brazil, ZIP code 29.270-030**
*** dan.bordim@gmail.com**

ABSTRACT: *The ballistic resistance and microwave absorption of a composite of aramid fabric impregnated with polyethylene glycol and hematite nanoparticles was investigated for different hematite concentrations between 0 and 17 wt%. Different damage and energy absorbing mechanisms during ballistic impact were identified: cone formation on the back face of the target, tensile failure of primary yarns and deformation of secondary yarns. In terms of energy absorption, the best results were achieved with 7 wt% hematite, while the smallest depth of penetration (DOP) was observed for a composite with 9 wt% hematite. A scanning electron microscope (SEM) image of the composite with 7% hematite after the ballistic test showed that the main energy absorption mechanism was deformation of secondary yarns. Microwave absorption was measured using the waveguide technique in the frequency range from 8 to 12 GHz. Results showed that the dielectric loss ε"/ε' is maximum for a concentration of 3% hematite, while the magnetic loss μ"/μ' is maximum for a concentration of 11 wt% hematite. A reasonable compromise between ballistic resistance and microwave absorption seems to be a composite with 7 wt% hematite.*

KEYWORDS: Radar absorption; Ballistic shielding; Ballistic impact; Shear thickening fluid.

RESUMO: *A resistência balística e a absorção de micro-ondas de um composto de tecido de aramida impregnado com polietilenoglicol e nanopartículas de hematita foram investigadas para diferentes concentrações de hematita entre 0 e 17% em peso. Foram identificados diferentes mecanismos de dano e de absorção de energia durante o impacto balístico: formação de cone na face posterior do alvo, falha de tração dos fios primários e deformação dos fios secundários. Em termos de absorção de energia, os melhores resultados foram obtidos com hematita a 7% em peso, enquanto a menor profundidade de penetração (DOP) foi observada em um composto com hematita a 9% em peso. Uma imagem de microscópio eletrônico de varredura (SEM) do compósito com 7% de hematita após o teste balístico mostrou que o principal mecanismo de absorção de energia foi a deformação dos fios secundários. A absorção de micro-ondas foi medida usando a técnica de guia de ondas na faixa de frequência de 8 a 12 GHz. Os resultados mostraram que a perda dielétrica ε"/ε' é máxima para uma concentração de 3% de hematita, enquanto a perda magnética μ"/μ' é máxima para uma concentração de 11% em peso de hematita. Um compromisso razoável entre a resistência balística e a absorção de micro-ondas parece ser um composto com 7 wt% de hematita.*

PALAVRAS-CHAVE: Absorção de radar; blindagem balística; impacto balístico; fluido de espessamento por cisalhamento.

1. Introduction

Since ancient times, mankind has sought the development of body protection against hazards and injuries. Animal skins, natural fibers and metallic materials such as bronze, iron and steel were used for this purpose throughout history. During the 20th century, natural fibers gave way to synthetic ones.

Modern armor is designed to protect against projectiles as well as against puncturing and cutting caused by sharp objects. They generally consist of a combination of metal, ceramics and fabrics. Fabrics are composed of high strength polymer fibers that provide added protection without compromising the mobility of soldiers, police officers and security personnel[1,2]. Advanced reinforcements were developed to improve the flexibility and reduce the weight of these fabrics using fewer layers and maintaining the same efficiency. These reinforcements are created by impregnating the fabrics with non-Newtonian fluids whose apparent viscosity vary with increasing stress[3-11].

The choice of magnetic nanoparticles for the production of a non-Newtonian fluid may add the property of being a Radar Absorption Material (RAM) to

the fabric. These materials are efficient attenuators of electromagnetic radiation at wavelengths used by radars, reducing the radar cross section of soldiers, automobiles, warships and military aircrafts. Teber et al.[12] used Ni-Co magnetic materials in polymeric composites as absorbers of X-band microwaves (8-12 GHz).

The purpose of this work was to study the armor reinforcement and radar absorption behavior[12-17] of a non-Newtonian fluid based on hematite. For this, mixtures of hematite nanoparticles with PEG-200 were produced with different concentrations of hematite. These blends were used to impregnate the aramid fabric; the ballistic resistance and the microwave absorption properties of the composite were evaluated for different hematite concentrations. In addition, damage and energy absorbing mechanisms during ballistic impact were investigated.

2. Materials and methods

2.1 Materials

The materials used in this work were ferric nitrate (Sigma-Aldrich, 98%), glycine (Sigma-Aldrich, 98.5%), 200 g/mol PEG (Honeywell Riedel-de Haën), absolute ethanol (Quimex, 93%), 0.28 mm thick aramid fabric with a 210 g/m² density [HY Networks (Shanhai)] and 1 inch thick MDF (Arauco do Brasil).

2.2 Sample Preparation

The hematite nanoparticles were synthesised using the combustion method with a 0.5 glycine/nitrate ratio[18,19]. Mixtures of PEG-200 with 0%, 3%, 5%, 7%, 9%, 11%, 13%, 15% and 17% hematite were sonicated for 30 min, diluted in 40 mL of ethanol, sonicated again for 30 minutes and used to impregnate two square pieces of aramid fabric with an area of 49 cm² in a 150 mm diameter watch glass. These pieces were pressed for 10 min at 3 ton/cm². Pressing the samples reduces the mass without decreasing ballistic resistance, because only non-impregnated fluid is removed. After this, the samples were oven dried at 79 °C for 24 h.

2.3 Experimental Methods

The hematite was characterized by X-ray diffraction using an Expert Pro Panalitical diffractometer with Cu Kα (1,5418 Å) radiation and TOPAS software based on the Rietveld method.

A Gunpower SSS air rifle with a noise suppressor Padrão Armas was used for the ballistic tests. The projectile was a 22-gauge lead shot with an estimated mass of 3.3g. The muzzle speed was measured using an Air Chrony MK3 ballistic chronograph with a precision of 0.15 m/s and the residual speed was measured using a ProChrono Pal ballistic chronograph with a precision of 0.31 m/s.

After the ballistic tests, images of samples with 7% hematite were obtained in a FEI Quanta FEG 250 SEM.

The electromagnetic characterization of the composites was performed by reflectivity/absorption measurements using the waveguide technique in the X-band of the electromagnetic spectrum (8 to 12 GHz). This device was coupled to an KEYSIGHT PNA-L Network Analyzer (model N5232A) with a frequency generator (300 kHz-20 GHz). The reference material used to evaluate the absorption efficiency of the composites was an aluminum plate, which reflects 100% of the incident radiation.

2.4 Relative mass M_c

The relative mass M_c was calculated using Eq. 1 to express the relative amount of impregnation of aramid by the fluid[11]:

$$M_c = (Mass\ of\ composite - Mass\ of\ aramid)/\ Mass\ of\ aramid. \quad (1)$$

2.5 Absorption energy (E_{abs})

In the energy absorption tests, the air rifle was positioned 5 m away from the target, which consisted of

a square sample attached to an MDF circular frame secured by a bench vise and aligned perpendicularly to the rifle. A ballistic chronograph was placed 10 cm away from the exit of the noise suppressor and another ballistic chronograph was placed 10 cm behind the composite to determine the residual speed of the projectile. The absorption energy was estimated using the equation

$$E_{abs} = M_p (v^2 - v_r^2)/2 \quad (2)$$

in which M_p is the projectile mass, v is the impact speed and v_r is the residual speed[20]. Pasquali et al.[21] showed that energy is absorbed by a target of thin woven fabric due to six absorption/dissipation mechanisms: cone formation on back face of the target ; tensile failure of primary yarns ; deformation of secondary yarns ; shear plugging ; delamination onset and growth; and matrix cracking[22,23].

2.6 Depth of penetration (*DOP*)

In the *DOP* tests, the air rifle was positioned 5 m away from the target, which consisted of a square sample attached with adhesive tape to an MDF plate and aligned perpendicularly to the rifle[24–29]. A noise suppressor was used to increase the stability of the projectile at the exit of the air rifle by reducing the swirling caused by the exhaust. MDF plates were used as bulkheads because MDF is a homogeneous material, flat and dense, without the grain of solid wood. The ballistic chronograph was placed 10 cm away from the exit of the noise suppressor. When the distance between the air gun and the target is small, as in this case, the impact speed may be replaced by the muzzle speed[30].

2.7 Merit factor

Since, in the ballistic test, the samples are thin and homogeneous, projectile deceleration a can be assumed to be constant. Applying Newton's second law

$$a = -F/M_p \quad (3)$$

where F is the force on the projectile, the Torricelli equation may be written in the form

$$v2 - v_r2 = 2\,(F/M_p)\,d \quad (4)$$

in which d is the distance traveled by the projectile. Replacing Eq. 2 in Eq. 4 and dividing by the relative mass M_c, *we have*

$$E_{abs}/(M_c\,d) = F/M_c \quad (5)$$

A merit factor *MF* was defined as the ratio shown in Eq. 5 with $DOP = d$:

$$MF = E_{abs}/M_c\,DOP \quad (6)$$

3. Results and discussion

3.1 X-ray diffraction

Figure 1 shows the X-ray diffraction pattern of the nanoparticles. The diffractogram showed 100% hematite, with 20 nm crystallite size and a GOF (Goodness of Fit) of 1.29.

Figure 1 - X-ray diffractogram of the nanoparticles.

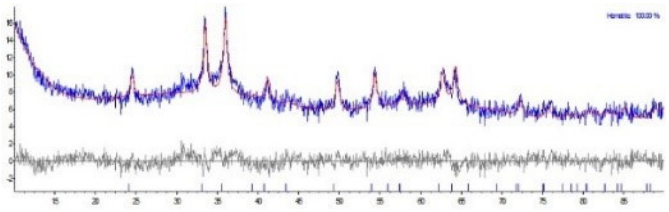

3.2 Ballistic tests

The ballistic tests consisted of measuring the energy absorbed by the composite and the depth of penetration (*DOP*) of a projectile on a medium density fiberboard (MDF) bulkhead.

All shots completely penetrated the sample. One shot was made in each experiment, and five experiments were performed for each composition.

Table 1 shows the composite relative mass (M_c), the absorption energy (E_{abs}), the depth of penetration (*DOP*) and the merit factor (*MF*) for all compositions. The energy absorbed is maximum for the samples with 7% hematite, while the *DOP* is minimum for samples with 9% hematite. This is attributed to the fact that the use of a bulkhead changes the mechanical behavior of the aramid fabric, favoring the breaking of primary fibers, which becomes an important energy absorption mechanism.

Table 1 - Average results of the ballistic tests.

COMPOSITE	M_c	E_{abs} (J)	DOP (mm)	MF (10-2) (J/mm)
A00	0.58 ± 0.07	5.70 ± 0.75	29.85 ± 0.35	32.72 ± 2.26
A03	0.62 ± 0.07	6.66 ± 0.91	27.75 ± 0.39	38.71 ± 3.00
A05	0.64 ± 0.06	6.69 ± 0.40	33.00 ± 0.43	31.68 ± 1.40
A07	0.57 ± 0.07	7.74 ± 0.58	28.58 ± 0.55	47.51 ± 2.78
A09	0.56 ± 0.06	6.01 ± 0.76	26.70 ± 0.40	40.20 ± 2.71
A11	0.53 ± 0.07	5.21 ± 0.37	29.92 ± 0.27	32.85 ± 1.67
A13	0.61 ± 0.06	6.51 ± 0.66	33.93 ± 0.55	31.45 ± 1.87
A15	0.58 ± 0.06	5.51 ± 0.54	27.97 ± 0.57	33.96 ± 2.12
A17	0.68 ± 0.09	6.14 ± 0.55	31.52 ± 0.50	28.65 ± 1.78

Figure 2 shows the dependence of the merit factor on hematite concentration. *MF* values were calculated using Eq. 2 with the values of $E_{abs,}$ *DOP* and M_c given in Table 1. The sample with the highest MF value was the one with 7% hematite (A07).

Figure 2 - Dependence of the merit factor on hematite concentration.

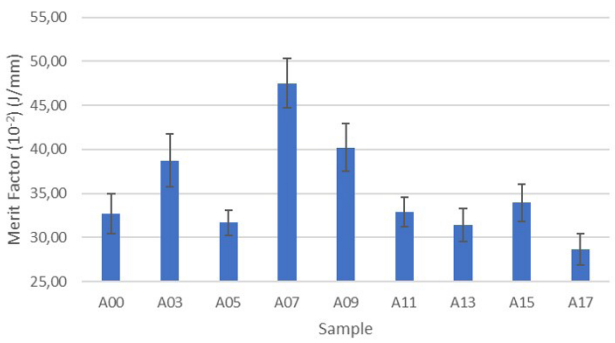

Figure 3 shows a sample with 7% hematite after the energy absorption test. One can see deformed primary and secondary yarns due to extended strain throughout the sample, suggesting a moderate pullout force.

Figure 3 - Sample with 7% hematite after the energy absorption test.

3.5 SEM images of an A07 sample

Figure 4 shows SEM images of a sample with 7% hematite (A07) before and after the ballistic test. Before the ballistic test (a), there is an excess of load that does not impregnate the aramid yarns and thus does not contribute significantly to ballistic resistance; and after the ballistic test (b), there is almost no excess of load, except in the bottom right of the image, where one can see clusters probably due to the impact[26]. The impact regions, which are not shown, are in the direction of the upper left corner of the images.

Figure 4 - SEM image of samples with 7% hematite (a) before and (b) after the impact.

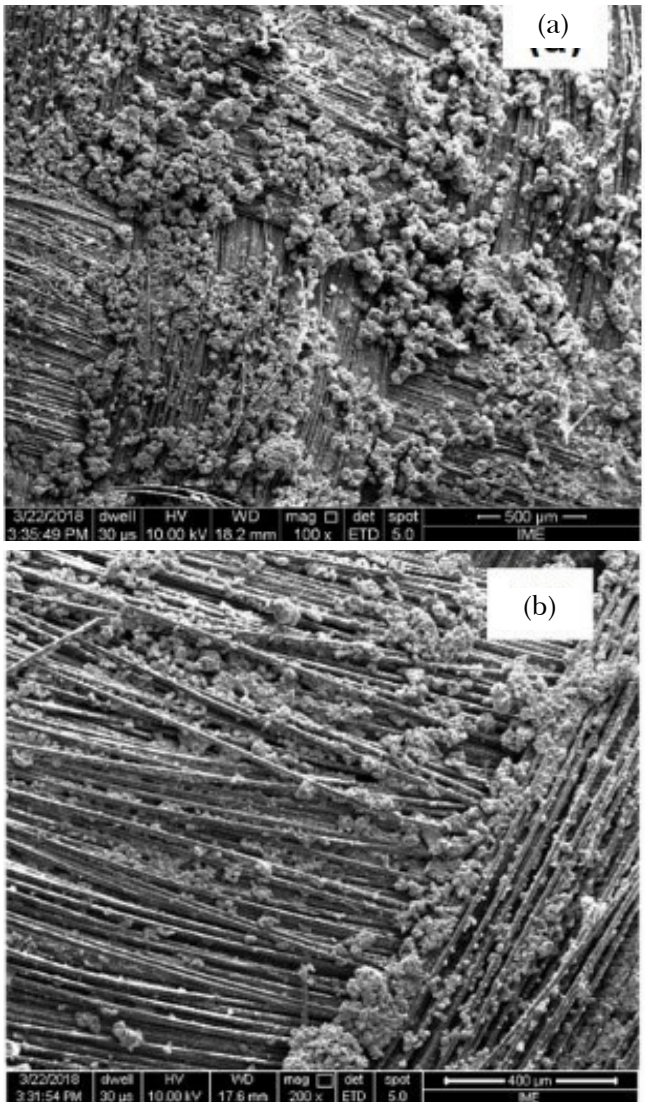

3.4 Reflectivity/absorption measurements

As shown in Figure 5, the dielectric loss ε"/ε' is maximum and the reflectivity loss is minimum for a concentration of 3% hematite. According to Huo et al.[31], this is due to the fact that for hematite concentrations larger than 3%, the skin depth becomes very small due to increasing conductivity and most of the electromagnetic wave is reflected. As shown in Figure 6, the magnetic loss μ"/μ' is maximum for 11 wt% hematite in the 8.2 to 11.6 GHz frequency range, but this effect is not enough to compensate the reflection loss caused by increasing conductivity, shown in Figure 5 (a). That is why, according to Figure 5 (b), it does not display the best performance in terms of reflectivity.

Figure 5 - (a) Dielectric and (b) reflectivity loss for pure aramid and aramid impregnated with an STF with 3%, 7%, 11% and 17% hematite.

(a)

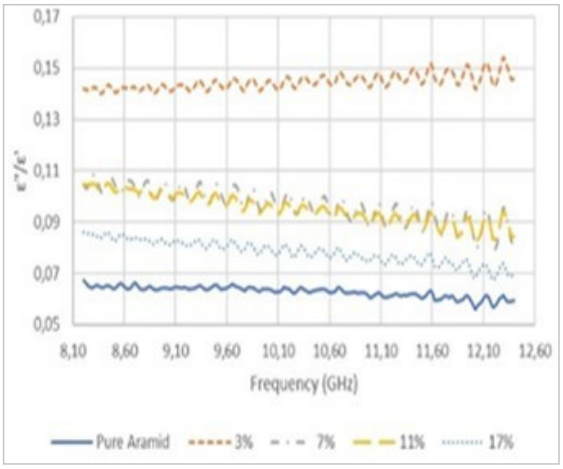

(b)

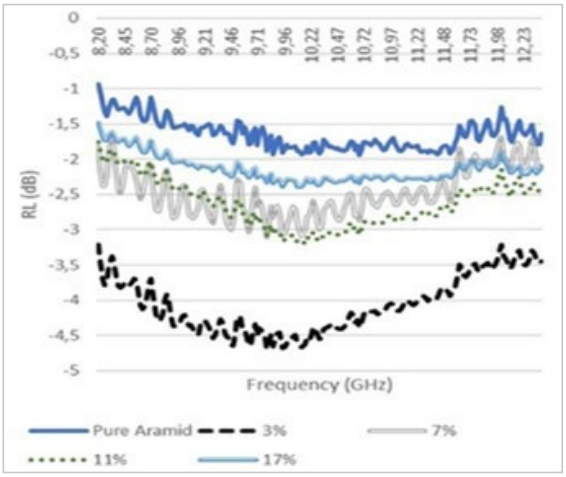

Figure 6 - Magnetic loss for pure aramid and aramid impregnated with an SFT with 3%, 7%, 11% and 17% hematite.

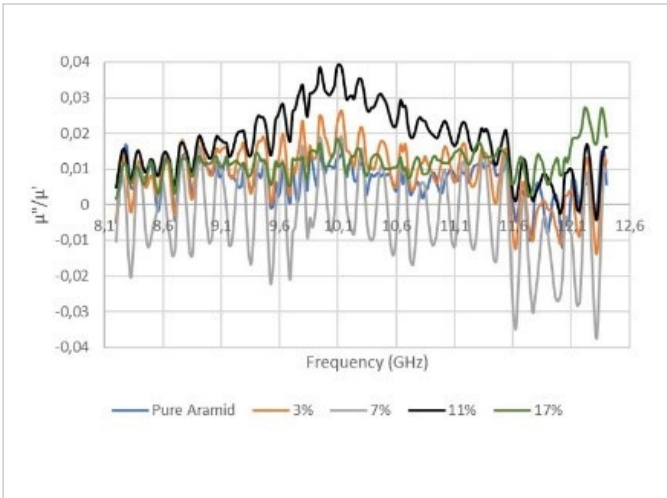

4. Conclusions

the composites with 7% hematite had the best ballistic behavior, while the composites with 3 wt% and 11% hematite had the best microwave absorption properties in terms of dielectric and magnetic loss, respectively. A reasonable compromise between ballistic resistance and microwave absorption seems to be using aramid fabric impregnated with 7 wt% hematite.

Acknowledgments

The authors thank CAPES (Coordination of Superior Level Staff Improvement) and CNPq (National Council for Scientific and Technological Development) for the financial support.

References

[1] CAVALLARO, P.V., Soft body armor: an overview of materials, manufacturing, testing, and ballistic impact dynamics, 1 August 2011, NUWC-NPT Technical Report 12,057
[2] EGRES, R. G. Jr., LEE, Y.S., KIRKWOOD, J. E., KIRKWOO, K. M., WETZEL E. D., WAGNER N.J. *Liquid armor: Protective fabrics utilizing shear thickening fluids*. In: IFAI INT. CONF. ON SAFETY AND PROTECTIVE FABRICS, 4. 2004, Pittsburgh. Conferência […]. Pittsburgh, 2004.
[3] EGRES, R.G. Jr., HALBACH, C.J., DECKER, M.J., WETZEL E.D., WAGNER N.J., Stab performance of shear thickening fluid (STF)-fabric composites for body armor applications, Proceeding of SAMPE 2005: New Horizons for Materials and Processing Technologies. Long Beach, CA., 2005.
[4] BARNES, H. A., HUTTON, J.F., WALTERS, K., An introduction to rheology, Rheology Series 3, Elsevier, 1989.
[5] MARANZANO, B.J., WAGNER, N.J., The effects of interparticle interactions and particle size on reversible shear thickening: Hard-sphere colloidal dispersions, J. Chem. Phys., v. 114, p. 10514, 2001.
[6] BRADY, J.F., The rheological behavior of concentrated colloidal dispersions, J. Chem. Phys., v.99, p. 567, 1993.
[7] KRISHNAMURTHY, L., WAGNER, N.J., Shear thickening in polymer stabilized colloidal dispersions, J. Rheol., v. 49, p. 1347, 2005.
[8] MARANZANO, B.J., NORMAN, J.W., The effects of particles size on reversible shear thickening of concentrated colloidal dispersions: Hard-sphere colloidal dispersions, J. Rheol., v. 45, p. 1205, 2001.
[9] GALINDO-ROSALES, F.J., RUBIO-HERNÁNDEZ, F.J., SEVILLA, A., An apparent viscosity function for shear thickening fluids, J. Non-Newtonian Fluid Mech., v. 166, p. 321, 2011.
[10] SUN, L. -L., XIONG, D. -S., XU, C.-Y., Application of shear thickening fluid in ultra high molecular weight polyethylene fabric, J. Appl. Polym. Sci, v. 129, p. 1922, 2013.
[11] MAJUMDAR, A., BUTOLA, B. S., SRIVASTAVA, A., Development of soft composite materials with improved impact resistance using Kevlar fabric and nano silica based shear thickening, Mater. Des., v. 54, p. 295, 2014.
[12] TEBER, A., UNVER, I., KAVAS, H., AKTAS, B., BANSAL, R., Knitted radar absorbing materials (RAM) based on nickel-cobalt magnetic materials, J. Mag. Mag. Mat, v. 406, p. 228, 2016.
[13] WU, Q.-M., RUAN, J.-M., HUANG, B.-Y., ZHOU, Z.C., ZOU J.-P., Rheological behavior of fumed silica suspension in polyethylene glycol, J. Cent. South Univ. Technol., v. 13, p. 1, 2006.
[14] GÜRGEN, S., LI, W., KUSHAN, M.C., The rheology of shear thickening fluids with various ceramic particle additives, Mater. Des., v. 104, p. 312,2016.
[15] DECKER, M.J., HALBACH, C.J., NAM, C.H., WAGNER, N.J., WETZEL, E.D., Stab resistance of shear thickening fluid (STF)-treated fabrics, Comp. Sci. Tech., v. 67, p. 565, 2007.

[16] EGRES, R.G., DECKER, M.J., HALBACH, C.J., LEE, Y.S., KIRKWOOD, J.E., KIRKWOOD, K.M., WAGNER, N.J. Stab resistance of shear thickening fluid(STF) Kevlar composites for body armor applications, Proceeding of the 24th Army Science Conference, Orlando, FL, 2004.
[17] DING, J., TRACEY, P.J., LI, W., PENG, G., WHITTEN, P.G. Review on shear thickening fluids and applications, Textiles and Light Industrial Science and Technology, v. 2, p. 161, 2013.
[18] DE BIASI, R.S., FIGUEIREDO, A.B.S., FERNANDES, A.A.R., LARICA, C., Synthesis of cobalto ferrite nanoparticles using combustion waves, Solid State Commun., v. 144, p. 15, 2007.
[19] CAO, Z., QIN, M., JIA, B., GU, Y., CHEN, P., VOLINSKY, A.A., QU, X., One pot solution combustion synthesis of highly mesoporous hematite for photocatalysis, Ceram. Int., v. 41, p. 2806, 2015.
[20] LEE, Y.S., WETZEL, E.D., WAGNER, N.J., The ballistic impact characteristics of Kevlar woven fabrics impregnated with a colloidal shear thickening fluid, J. Mater. Sci., v. 38, p. 2825, 2003.
[21] PASQUALI, M., TERRA, C., GAUDENZI, P., Analytical modelling of high-velocity impacts on thin woven fabric composite targets, Compos. Struct., v. 131, p. 951, 2015.
[22] NAIK, N.K., SHRIRAO, P., Composite structures under ballistic impact, Compos. Struct., vol. 66, p. 579, 2004.
[23] NAIK, N.K., SHRIRAO, P., REDDY, B.C.K., Ballistic impact behaviour of woven fabric composites: Formulation, Int. J. Impact Eng., vol. 32, p. 1521, 2006.
[24] ALMUSALLAM, T.H., SIDDIQUI, N.A., IQBAL, R.A., ABBAS, H., Response of hybrid-fiber reinforced concrete slabs to hard projectile impact, Int. J. Impact Eng., v. 58, p. 17, 2013.
[25] WANG, J., CALLINAN, R., Residual strengths of composite structures subjected to ballistic impact, Compos. Struct., v. 117, p. 423, 2014.
[26] JORDAN, J.B., NAITO, C.J., Calculating fragment impact velocity from penetration data, Int. J. Impact Eng., v. 37, p. 530, 2010.
[27] BACKMAN, M.E., GOLDSMITH, W., The mechanics of penetration of projectiles into targets, Int. J. Eng. Sci., v. 16, p. 1, 1978.
[28] CARLUCCI, D.E.; JACOBSON, S.S. Ballistics: theory and design of guns and ammunition. Boca Raton [Florida]: CRC, 2008. 496 p. ISBN 1420066180.
[29] ANDERSON JR., C.E., Analytical models for penetration mechanics: A Review, Int. J. Impact Eng., v. 108, p. 3, 2017.
[30] VILLANUEVA, G.R.; CANTWELL, W.J. The high velocity impact response of composite and FML-reinforced sandwich structures, Comp. Sci. Tec., v. 64, p. 35-54, 2004.
[31] HUO J., WANG L., YU H., Polymeric nanocomposites for electromagnetic wave absorption, J. Mater. Sci., v. 44, p. 3917, 2009.